IOP Conf. Series: Materials Science and Engineering **380** (2018) 012011 doi:10.1088/1757-899X/380/1/012011

Effect of Inhibitors on the Crystallization and Magnetic Properties of Nanocrystalline Alloys

V S Tsepelev[1], Yu N Starodubtsev[1,2] and N P Tsepeleva[1]

[1]Boris Yeltzin Ural Federal University, 19 Mira str., Yekaterinburg, 620002, Russia
[2]Gammamet Research and Production Enterprise, 92 Tatishchev str., Yekaterinburg, 620028, Russia

E-mail: v.s.tsepelev@urfu.ru

Abstract. In the paper, the crystallization process of nanocrystaline alloys $Fe_{73.5}Cu_1M_3Si_{13.5}B_9$ where M = Nb, W, Mo, V, Cr and the physical origin of different efficiency of impact that inhibitors exert on the structure and magnetic properties has been investigated. It is shown that the structure formed at the peak temperature of the crystallization process is close to the optimal one and ensures high values of magnetic permeability. The efficiency is directly related to the solubility of inhibitory elements in αFe, which in turn affects the diffusivity of atoms. Upon slow migration of grain boundaries, the inhibitory atoms with lower diffusivity, being concentrated near the front of moving boundary, provide stronger drag.

1. Introduction

Nowadays, nanocrystalline soft magnetic materials are widely used in the manufacture of magnetic systems of transformers, electric reactors, chokes, and other devices operated at frequencies up to 10 MHz [1]. High magnetic permeability and low magnetic losses are provided by the nanosized crystal structure of the materials [2, 3]. In the material of the Finemet type with the chemical composition of $Fe_{73.5}Cu_1Nb_3Si_{13.5}B_9$, the average size of Fe-Si crystallites is of the order of 10 nm [4]. The chemical composition of the alloy includes elements that provide realization of an amorphous structure upon quenching (Si, B), as well as elements favoring the formation of nanosized grains in the course of heat treatment (Cu, Nb) [5, 6]. In this alloy, Nb is used for inhibition of grain growth. Other elements can also find their application as inhibitors [7–10], and they can be arranged in the order of increasing the efficiency of grain refinement: Cr, V, W = Mo, Nb = Ta, Zr.

Nanocrystalline soft magnetic alloys are the subject-matter of many physical researches. Of special interest is the process of crystallization from the amorphous solid state and its impact on the magnetic properties of the material, as well as the means of controlling this process. To investigate the process of crystallization, different methods are employed. One of such methods is thermomagnetic analysis. Within the classical thermomagnetic analysis, the temperature dependence of the saturation magnetization is determined [11, 12]. In the alloys with high magnetic permeability, new results can be obtained by analyzing changes in the initial permeability in the course of heat treatment.

In this paper, the thermomagnetic analysis of the nanocrystalline soft magnetic alloys was performed. The physical origin of different efficiency of impact that inhibitors exert on the structure and magnetic properties of nanocrystaline alloys $Fe_{73.5}Cu_1M_3Si_{13.5}B_9$ where M = Nb, W, Mo, V, Cr has been studied.

2. Experimental

The $Fe_{73.5}Cu_1M_3Si_{13.5}B_9$ alloys where M = Nb, W, Mo, V, Cr were melt in a vacuum induction furnace. A 25 μm thick and 10 mm wide ribbon with the amorphous structure was produced by the planar flow casting process. The ribbon was wound up onto ring-type cores with the 32 mm outer diameter and 20 mm inner diameter. The thermomagnetic analysis was performed with the simultaneous recording of the temperature inside the core by a thermocouple and the inductance of the winding wound over the core. For the analysis, 7 cores of $Fe_{72.5}Cu_1Nb_2Mo_{1.5}Si_{14}B_9$ were wound with one and the same ribbon sequentially, one after another. In the course of heat treatment at the temperature of 813 K the cores were taken out of the furnace and quickly cooled at the rate of 70 K/min to fix the structure at different stages of the crystallization, the temperature and inductivity being continuously recorded at the specified time moments shown in Figure 1 by digits 1 – 7. The initial permeability μ was calculated based on the inductance measurements at 1 kHz. Parameters of the DC magnetization curve and hysteresis loop were determined by means of point-by-point DC testing [13]. Specific magnetic losses $P_{0.2/20}$ were measured at the frequency of 20 kHz with the magnetic induction B_m = 0.2 T.

3. Results and discussion

Figure 1 shows the in-time changes in the temperature and permeability of a core made of the alloy $Fe_{72.5}Cu_1Nb_2Mo_{1.5}Si_{14}B_9$ upon crystallization in the furnace at the temperature of 813 K. The temperature curve enables determining the initial rate of heating the core prior crystallization, V_0 = 5 K/min (a linear portion up to point 1), the onset temperature of crystallization T_{cr} = 793 K at point 1 (the starting point of the nonlinear temperature growth), the point of maximal temperature increment – 2, the maximal rate V_m 39 K/min of heating the core after point 2, and the peak temperature in the process of crystallization T_m = 854 K at point 3. On the magnetic permeability curve, it is possible to pick out point 4 that corresponds to the beginning of the permeability growth, the portion of the maximal growth rate to point 5, the onset temperature of the maximal permeability growth T_μ = 826 K, the peak value of permeability μ_m = 4800 at point 5, the point of maximal decrease 6, and the stabilized value μ_{st} = 840 at point 7 after completing the crystallization process.

From Figure 1, it is seen that the growth of permeability in the course of crystallization is non-monotonous. After reaching the peak value μ_m, the permeability decrease in time is almost just as quick, going to the steady value μ_{st}. Besides, it follows from Figure 1 that the permeability peak μ_m is 4 minutes behind the temperature peak (T_m).

Table 1 contains data on the permeability $\mu_{0.08}$, the maximum permeability μ_{max}, coercivity H_c, and magnetic losses $P_{0.2/20}$ for the cores the heat treatment of which was interrupted at characteristic time instants depicted by figures 1 – 7 in Figure 1. It follows from Table 1 that of the whole series only cores 1 and 2 are out of line; they correspond to the initial (1) and advanced (2) stages of crystallization, at which the magnetic properties are rather low. Starting from core 3 that corresponds to the peak temperature T_m and further on, for all the subsequent stages, the magnetic properties of the cores are virtually the same. The results of magnetic measurements indicate that after reaching the peak temperature T_m, the alloy structure is nearly optimal.

The bulk of sample 1 is occupied mainly by the amorphous phase in which a crystal phase starts forming. In the micro-diffraction pattern, broad smeared rings are seen and, at their background, the emerging point reflections of the crystal phase. The average size of the grains formed makes up 6 nm. The maximum of the size distribution corresponds to 2 nm; these grains can be ascribed to the crystal phase nuclei. There is also another maximum at about 8 nm in the histogram. Samples 3 and 7 are virtually undistinguished in structure. The micro-diffraction pattern shows that the process of crystallization is completed with the formation of solid solution of silicon in α-Fe. In the electron diffraction patterns, a small amount of the Fe_3Si phase is detected. The histograms of the size distribution show up that the number of the crystallization nuclei in samples 3 and 7 is noticeably decreased compared to sample 1. The main maximum is located at about the average size which is 10 nm, and the second maximum appears to be close to 15 nm. Applying Scherrer's method, the maximum in the vicinity of 10 nm is ascribed to crystals of the α-Fe(Si) solid solution and that in the vicinity of 15 nm, to the Fe_3Si phase.

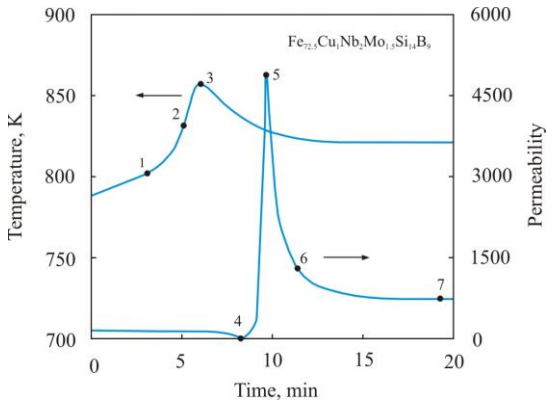

Figure 1. In-time changes of temperature and permeability of the core made from the $Fe_{72.5}Cu_1Nb_2Mo_{1.5}Si_{14}B_9$ alloy in the course of crystallization.

Table 1. Magnetic properties of cores made of the $Fe_{72.5}Cu_1Nb_2Mo_{1.5}Si_{14}B_9$ alloy at 300 K after heat treatment interrupted at different stages of the crystallization process.

Core number	Permeability, $\mu_{0.08}$	Maximal permeability, μ_{max}	Coercivity, H_c, A/m	Magnetic losses $P_{0.2/20}$, W/kg
1	5600	278000	1.25	15.0
2	11700	342000	0.85	8.7
3	67600	521000	0.50	3.3
4	79100	527000	0.55	2.8
5	67000	678000	0.45	4.2
6	73900	575000	0.50	3.2
7	71900	612000	0.50	3.5

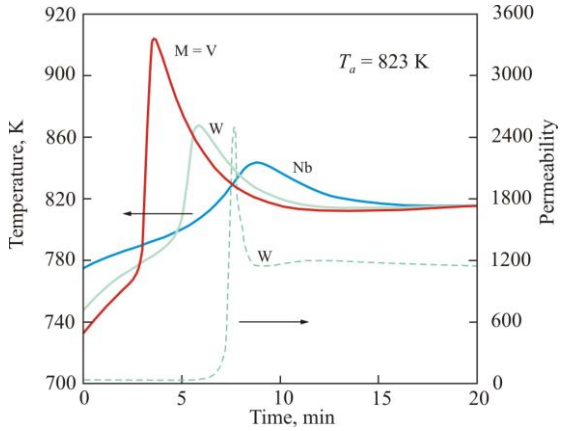

Figure 2. In-time changes of temperature and permeability in the course of crystallization of the core made from the $Fe_{73.5}Cu_1M_3Si_{13.5}B_9$ alloy, where M = Nb, W, V.

Figure 2 displays the in-time change of temperature of cores made from $Fe_{73.5}Cu_1M_3Si_{13.5}B_9$, where M = Nb, W, V in the course of heating in furnace, the temperature of which was kept T_a = 823 K. The temperature curves for different alloys are presented on the same time scale in the range of crystallization. As an example, the dashed line in Figure 2 shows a time dependence of permeability matching the corresponding temperature curve for the $Fe_{73.5}Cu_1W_3Si_{13.5}B_9$ alloy. From the temperature

curves there were determined the Curie temperatures of the alloys in the amorphous state T_C, the onset temperature of crystallization T_x, the maximal temperature of the core heating in the course of crystallization T_{max}, and the maximal rate of elevating temperature in the course of crystallization V_{max}. The temperature at which permeability starts growing in the course of crystallization T_μ was determined from the corresponding permeability changes. This temperature can be taken as the Curie temperature of the arising crystalline phase with the composition corresponding to the initial stage of crystallization. All numerical values of the above-listed parameters for different alloys are shown in Table 2. Additionally, the table contains data on the core permeability after annealing, i.e., after crystallization and cooling to 300 K.

Table 2. Parameters of crystallization for the $Fe_{73.5}Cu_1M_3Si_{13.5}B_9$ alloys with the grain growth inhibitors M = Nb, W, Mo, V, Cr.

$Fe_{73.5}Cu_1M_3Si_{13.5}B_9$ alloys with grain growth inhibitors M	Temperature, K				Temperature growth rate V_{max}, K/min	Permeability μ after annealing at 823 K
	T_C	T_x	T_{max}	T_μ		
Nb	600	799	843	822	15	85000
W	597	788	867	847	103	65000
Mo	594	783	868	862	157	75000
V	623	769	922	–	306	1000
Cr	621	763	921	–	445	150

As follows from the Table 2, the maximal permeability is gained on the alloy containing Nb. The W and Mo inhibitors are also efficient for achievement of high permeability, unlike V and Cr. The course of crystallization in the alloys with various inhibitors drastically differs. In the alloy with Nb, the temperature peak is smoothened to a maximal degree, and the process of crystallization is featured by the minimal values of the peak temperature T_{max} = 843 K and the rate of elevating temperature V_{max} = 15 K/min and maximal value of the onset temperature of crystallization T_x = 799 K. The numerical values of T_{max} and V_{max} gradually grow, whereas T_x lowers from row to row sequentially for Nb, W, Mo, V, Cr. The average grain size sequentially grows in the series of inhibitors Nb, W, Mo, V, Cr. In the alloy with Nb the average grain size is 8 mm and no grains larger than 30 nm were detected. In the alloys with V and Cr, the average grain size exceeds 20 nm, the coarsest grains being up to 80 nm.
To discuss the whole bulk of the results obtained, let us present the data on inhibitory elements taken from different sources [14–17]. In Table 3 there are collected solubility of elements in αFe at 1000 K; metallic radius of atoms r_i, relative radius according to the criterion after the Hume-Rothery rule $(r_i – r_{Fe})/r_{Fe}$, where the metallic radius of iron r_{Fe} = 126 pm; and activation energy of diffusion in в αFe.

Table 3. Properties of inhibitors.

Grain growth inhibitors	Solubility in αFe at 1000K, at% [14, 15]	Metallic radius r_i, pm [16]	Hume-Rothery rule $(r_i–r_{Fe})/r_{Fe}$, %	Activation energy for diffusion in αFe D, kJmol^{-1} [17]
Nb	0.12	146	15.9	299
W	1.0	139	10.3	–
Mo	2.5	139	10.3	282
V	unlimited	134	6.3	274
Cr	unlimited	128	1.6	267

All inhibitory elements in Table 3 are arranged in the order of increasing solubility in αFe. According to the Hume-Rothery rule [18], the solubility limit is reached when the atomic radius of the solute is by 15 % higher than that of the solvent. In accordance with this criterion, Nb atoms are virtually soluble in αFe, whereas the solubility of other elements rises in array Nb, W, Mo, V, Cr. With an increase in solubility of elements, the activation energy of diffusion consistently lowers.

The process of crystallization is accompanied by an increase in the volume of crystalline phase at the expense of migration of grain boundaries. Impurity (inhibitory) atoms interact with a moving boundary so that the boundary either carries these atoms with the velocity of its motion not exceeding that of atomic diffusion or drives off from them [19]. At a small velocity of the boundary migration, atoms with lower diffusion mobility, concentrating near the front of the moving boundary and remaining undissolved in the crystalline phase, provides a stronger drag.

Thus, the drag effect of the grain boundaries in the process of crystallization sequentially weakens in the array Nb, W, Mo, V, Cr, which manifests itself in the lowering of the crystallization-onset temperature T_x, as well as in the increase in the rate of elevating temperature V_{max} and in the peak temperature of the core heating T_{max}. The change in the velocity of migration of grain boundaries affects the extent of the crystallization process. Thus, the alloy with Nb has a structure characteristic of the initial stage of crystallization, namely, fine grains with the presence of a significant amount of grains 2 nm in size, and a predominant volume fraction of the αFe-Si solid solution. At the subsequent stages of crystallization, the grain size grows, the fraction of the stable Fe_3Si phase increases, and then, iron borides precipitate.

4. Summary

In the paper, the crystallization process of nanocrystaline alloys $Fe_{73.5}Cu_1M_3Si_{13.5}B_9$ where M = Nb, W, Mo, V, Cr and the physical origin of different efficiency of impact that inhibitors exert on the structure and magnetic properties has been investigated. It is shown that the structure formed at the peak temperature of the crystallization process is close to the optimal one and ensures high values of magnetic permeability. The efficiency of inhibitors is directly related to the solubility of inhibitory elements in αFe, which in turn affects the diffusivity of atoms. Upon slow migration of grain boundaries, the inhibitory atoms with a lower diffusivity, being concentrated near the front of moving boundary, provide a stronger drag. The weakening of the effect manifests itself in the lowering of the onset temperature of crystallization, as well as in the increase in the rate of elevating temperature and in the peak temperature of the core heating.

5. Acknowledgments

This work was supported by the Scientific researches of higher education institutions within the State task of the Russian Federation No. 4.9541.2017/8.9.

6. References

[1] Y Yoshizawa, *Handbook of Advanced Magnetic Materials*, Properties and Applications Vol. 4, ed D J Sellmyer and D Shindo, Springer (2006), pp. 124 – 158.
[2] Y Yoshizawa, S Oguma and K. Yamauchi J, *Appl. Phys*. 64 (1988), pp. 6044 – 6046.
[3] G Herzer, *IEEE Trans. Magn*. 25 (1989), pp. 3327 – 29.
[4] G Herzer, *Handbook of Magnetic Materials*, ed. K H J Buschow, 10 (1997), pp. 415 – 462.
[5] K Hono, D H Ping, M Onhuma and H Ondera, *Acta Mater*. 47 (1999), pp. 997 – 1006.
[6] W Lefebvre, S Morin-Grognet and F Danoix, *J. Magn. Magn. Mater*. 301 (2006) pp. 343 – 351.
[7] Y Yoshizawa and K Yamauchi, *Mater. Sci. Eng*. A133 (1991), pp. 176–179.
[8] M Müller and N Mattern, *J. Magn. Magn. Mater*. 136 (1994) 79–87.
[9] V A Peña Rodríguez, J F Regalado, E Baggio-Saitovitch and E C Passamani, *J. Alloys Comp*. 379 (2004), pp. 23–27.
[10] Wei Lu, Junwei Fan, Yuxin Wang and Biao Yan, *J. Magn. Magn. Mater*. 322 (2010), pp. 2935–37.

[11] J M. Borrego, C F Conde, A Conde and Phil. *Mag. Lett*. 80 (2000), pp. 359 – 365.
[12] J M Silveyra, E Illeková, P Švec, D Janičkovič, A Rosales-Rivera and V J Cremaschi, *Phys*. B 405 (2010), pp. 2720 – 25.
[13] S Tumanski, *Handbook of magnetic measurements*, CRC Press, Taylor&Francis Group (2011).
[14] O Kubaschewski, Iron–binary phase diagrams, Springer, 1982.
[15] Diagrams of binary metallic systems, 2, ed. N P Lyakishev, Moscow, 1997.
[16] N N Greenwood and A. Earnshaw, *Chemistry of the elements*, Butterworth-Heinemann, 1998.
[17] N Oono, H Nitta and Y Iijima, *Mater. Trans*. 44 (2003), pp. 2078–83.
[18] W Hume-Rothery and G V Raynor, *The structure of metals and alloys*, The institute of metals, 1962.
[19] G Gottstein and L S Shvindlerman, *Grain boundary migration in metals: thermodynamics, kinetics, applications*, CRC Press, 2010.